SCIENCE CHINA
Technological Sciences

Progress of Projects Supported by NSFC

December 2012 Vol.55 No.12: 3359–3369
doi: 10.1007/s11431-012-5025-0

On the thrust performance of an ionic polymer-metal composite actuated robotic fish: Modeling and experimental investigation

WANG TianMiao[1], SHEN Qi[1*], WEN Li[2] & LIANG JianHong[1]

[1] *Robotic Institute, School of Mechanical Engineering and Automation, Beihang University, Beijing 100191, China;*
[2] *Museum of Comparative Biology, Harvard University, 26 Oxford St., Cambridge, MA 02138, USA*

Received April 21, 2012; accepted July 9, 2012; published online September 10, 2012

In this paper, we theoretically predict and experimentally measure the thrust efficiency of a biomimetic robotic fish, which is propelled by an ionic polymer-metal composite (IPMC) actuator. A physics-based model that consists of IPMC dynamics and hydrodynamics was proposed, and simulation was conducted. In order to test the thrust performance of the robotic fish, a novel experimental apparatus was developed for hydrodynamic experiments. Under a servo towing system, the IPMC fish swam at a self-propelled speed where external force is averagely zero. Experimental results demonstrated that the theoretical model can well predict the thrust efficiency of the robotic fish. A maximum thrust efficiency of 2.3×10^{-3} at 1 Hz was recorded experimentally, the maximum thrust force was 0.0253 N, recorded at 1.2 Hz, while the maximum speed was 0.021 m/s, recorded at 1.5 Hz, and a peak power of 0.36 W was recorded at 2.6 Hz. Additionally, the optimal actuation frequency for the thrust efficiency was also recorded at the maximum self-propelled speed. The present method of examining the thrust efficiency may also be applied to the studies of other types of smart material actuated underwater robots.

biomimetic robotic fish, hydrodynamic modeling, thrust efficiency measurement, ionic polymer-metal composites

Citation: Wang T M, Shen Q, Wen L, et al. On the thrust performance of an ionic polymer-metal composite actuated robotic fish: Modeling and experimental investigation. Sci China Tech Sci, 2012, 55: 3359–3369, doi: 10.1007/s11431-012-5025-0

Nomenclature

U	Velocity of the IPMC fish
s	Laplace variable
$w(x, t)$	Amplitude of IPMC tail at point x (m)
x	The spatial coordinate along the length of the beam (m)
S	Characteristic cross-sectional area of fish body (m^2)
$\overline{(\cdot)}$	Mean value
C_D	Drag coefficient
ρ_w	Density of the fluid (kg/m^3)
m	Virtual mass density at the end of tail (kg)
S_c	Width of the tail at the end of tail (m)
β	Virtual-mass coefficient parameter
Y	Young's modulus of IPMC (Pa)
I	The moment of inertial of the beam (m^4)
μ	The mass per unit length of the beam (kg/m)
$F(x,s)$	The external force per unit length acting on the beam (N/m)
x'	Variable in Green's function related with x
t	Time (s)
W	Width of the beam (m)
L	Length of the IPMC beam (m)
h	Half thickness of the IPMC beam (m)
ω	Radial frequency (rad/s)
$\Gamma_1(\omega)$	Dimensionless hydrodynamic function of the IPMC beam
$G(x,x',s)$	Green's functions
$V(s)$	Applied voltage on IPMC (V)
α_0	Electromechanical coupling constant (J/C)
d	Ionic diffusivity (m/s)
R	Gas constant (J/mol K)
F	Faraday's constant (C/mol)
T_a	Absolute temperature (K)
C^-	Anion concentration (mol/m^3)

*Corresponding author (email: eric.shen1987@gmail.com)

r_1	Electrode resistance per unit length in the length direction (Ω/m)
r_2	Electrode resistance per unit length in the thickness direction (Ω m)
ΔV	Volumetric change (m^3)
κ_e	Effective dielectric constant of the polymer (F/m)
R_p	Through-polymer resistance per unit length (Ω m)

1 Introduction

A number of biomimetic underwater robots have been developed [1–6]. The use of smart material has also applied to the development of biomimetic underwater robots, such as piezoelectric actuator, shape memory actuator and polymer actuator [7–9]. Ionic polymer-metal composite (IPMC) is one of the promising smart materials for biomimetic underwater propulsion [10, 11]. It is made of ionic polymer membrane with plated gold as electrodes on both sides chemically. If one provides an electric field through their thickness, it would bend accordingly. On the other hand, a detectable voltage can be generated if the material is subjected to a mechanical deformation. It has the advantage of low activation voltage (1–2 V), limited power consumption, silent operation, and high flexibility. Therefore the ionic polymer metal composite provides the possibility for developing a low-noise, micro-size, flexible biomimetic robot.

Many IPMC based biomimetic underwater robots have been developed, such as robotic rajiform, robotic fish, snake-like robot, etc. [12–15]. Yim et al. [16] proposed an analytical model of IPMC actuator dynamic characteristics for the application of underwater propulsor, which could be used for modeling a single- or multi-segment IPMC actuator that operates in water. However, the theoretical model was only simulated without experimental validation. Tan presented the speed model for IPMC-propelled robotic fish and experimentally tested it [17–19]. Porfiri developed a modeling framework for motion prediction of biomimetic underwater vehicles propelled by IPMC [20]. The hydrodynamics of an IPMC beam was investigated using numerical computation and digital particle image velocimetry (DPIV) [21, 22]. Nevertheless, the IPMC beam was clamped in water and was not tested as a freely swimming underwater robot. With regard to the small robots, the swimming efficiency is essential for power limitation. To date, few studies have reported the thrust efficiency of the IPMC actuated underwater robot.

The first goal of this paper is to provide a theoretical thrust efficiency model for IPMC actuated robotic fish. The model includes the hydrodynamics such as added mass and hydrodynamic force. The elongated body theory of Lighthill [23] was applied to the thrust performance evaluation of the swimming robot, in which the thrust efficiency of the robotic fish is related to the bending displacement and the slope of the IPMC tail end. Through deriving the solution to a forth-order partial differential equation, the beam dynamics of IPMC in fluid was obtained. Thus, the speed model and the thrust efficiency model of the IPMC fish were achieved. Compared with the speed model in ref. [18], which contains infinite terms and uses first three terms for approximation, the speed model presented in this paper consists of finite terms and is simplified. More importantly, this paper provides the thrust efficiency model.

The second goal of this paper is to experimentally study the thrust efficiency of robotic fish with different IPMC tails. Firstly, displacement experiments were conducted to identify the model parameters and validate the theoretical model. Most of the parameters in the proposed model were identified through fundamental physical properties of IPMC and its geometric dimensions. Secondly, we used a novel approach to simultaneously measure thrust force and self-propelled speed of the robotic fish. Based on this method, the robotic fish can swim under self-propulsive condition rather than external constraints of the towing system. The thrust force, power consumption in the fluid, steady swimming speed of the robotic fish were recorded. Furthermore, thrust efficiency was calculated based on the experimental data. Additionally, the experimental results were compared with the theoretical results for different frequencies.

The rest of this paper is organized as follows. The robotic fish is described in Section 2. The dynamic model is presented in Section 3. Experiment validation and comparison with model prediction are presented in Sections 4 and 5. Section 6 is the conclusion.

2 Description of the IPMC robotic fish

This section provides a brief introduction to the robotic fish design. Figure 1 shows the robotic fish prototype which consists of three parts: 1) the rigid body shell which is the fish body, 2) the IPMC which is its "muscle", and 3) the plastic piece that mimics the tail fin. The body shell closely resembling an ellipsoidal shape was designed in SolidWorks. It was fabricated with nylon plastics by using 3D printer and covered with black matt resin varnish so as to obtain a smooth surface. Its shape was designed according to the body proportion of yellow croaker (*Pseudosciaena*

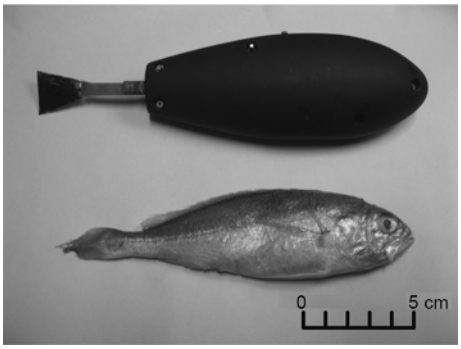

Figure 1 Prototype of the robotic fish.

crocea) to make the body streamlined. The IPMC is attached to the body by small rectangular conductive copper plates acting as a clamp. The fin is attached to the end of the IPMC to produce a larger force.

The battery units (two 3.7 V in series) and the electronics are implemented within the shell. Inspired by the motor design, the control of IPMC is based on H-bridge utilizing L298N, which enables convenient I/O control and large current. A counterweight is put in the bottom of the fish to achieve buoyancy and enhance stability of the rolling and pitching directions. The robotic fish was experimentally studied both for swimming underwater and the servo towing system under self-propelled condition. The fish has a total length of 144 mm without the tail, 52.5 mm in height and 37.5 mm at its widest point. The total weight of the robotic fish approximates 180 g.

3 Thrust efficiency model of the robotic fish

The main purpose in this section is to build the model of the actuation of IPMC beam and its hydrodynamic thrust efficiency model. In the following subsections, we will first introduce Lighthill's elongated body theory. Then IPMC beam dynamics in fluid is discussed. It is followed by a detailed analysis on the IPMC actuation and hydrodynamic force acting on the beam and passive fin. Through combing Lighthill's theory on elongated body and the beam's hydrodynamics, the thrust efficiency model of the IPMC-propelled robotic swimmer is obtained.

3.1 Lighthill's theory on elongated body

The Lighthill's elongated theory applies to a fish or a swimming mammal whose cross-section gradually varies along its length and changes slowly [23]. The robotic fish in Section 2 is thus elongated and can be dealt with Lighthill's theory. It is assumed that the IPMC tail satisfies the following restrictions: 1) The nominal width of the tail is greatly exceeded by its length; 2) the amplitude of the tail is far smaller than its length scale, so that the tail is supposed to bend periodically at x denoted by $w(x, t)$ (see Figure 2).

At steady swimming, the swimming speed of IPMC fish reaches equilibrium at a constant value $\overline{U}$. The swimming speed $\overline{U}$ of IPMC fish can be predicted [18] as

$$\overline{U}=\left[\sqrt{\frac{m\cdot\overline{\left(\frac{\partial w(x,t)}{\partial t}\right)^2}}{C_{\mathrm{D}}\rho_{\mathrm{w}}S+m\cdot\overline{\left(\frac{\partial w(x,t)}{\partial x}\right)^2}}}\right]_{x=L}, \tag{1}$$

where $x=L$ denotes the end of the tail, and m is expressed as $m=\pi S_{\mathrm{c}}^2\rho_{\mathrm{w}}\beta/4$.

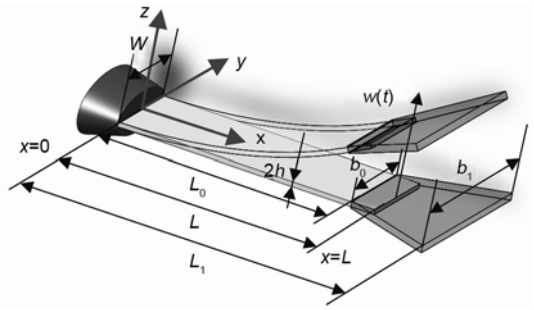

Figure 2 Geometric definitions for the model of IPMC.

The swimming efficiency of a real fish is defined as the ratio of the actual power (contributed to the propulsion) to the total amount of the power consumed by the fish [24]. In robotics area, there is a similar measure of swimming efficiency, which is defined by the ratio between useful power and the total power input in the fluid [25]. In this paper, we adopt the Froude efficiency index based on Lighthill's elongated body theory [26]. The expression of the thrust efficiency is donated as

$$\eta=\frac{\overline{TU}}{\overline{W}}=1-\frac{1}{2}\left[\frac{\overline{\left(\frac{\partial w(x,t)}{\partial t}+\overline{U}\frac{\partial w(x,t)}{\partial x}\right)^2}}{\overline{\frac{\partial w(x,t)}{\partial t}\left(\frac{\partial w(x,t)}{\partial t}+\overline{U}\frac{\partial w(x,t)}{\partial x}\right)}}\right]_{x=L}. \tag{2}$$

The expressions of $\frac{\partial w(x,t)}{\partial t}$ and $\frac{\partial w(x,t)}{\partial x}$ will be obtained henceforth to gain the speed model and thrust efficiency model.

3.2 Dynamics of IPMC beam in fluid

In this subsection we will discuss the IPMC beam dynamics in fluid. The governing equation for the IPMC dynamic deflection $w(x, t)$ of the beam can be denoted as [27]

$$YI\frac{\partial^4 w(x,t)}{\partial x^4}+\mu\frac{\partial^2 w(x,t)}{\partial t^2}=F(x,t). \tag{3}$$

We convert eq. (3) into the Laplace domain to obtain

$$\frac{YI}{L^4}\frac{\partial^4 w(x,s)}{\partial x^4}+\mu s^2 w(x,s)=\widetilde{F}(x,s), \tag{4}$$

where x is non-dimentionized by the length of beam L. The spatial variable x in eq. (4) refers to its scaled quantity and this convention will be applied henceforth.

According to the dynamic of IPMC beam in the liquid, the applied force on the beam consists of two components, the hydrodynamic force acting on the IPMC beam at point x $\widetilde{F}_{\mathrm{hydro}}(x,s)$ and the driving force due to the actuation of

IPMC at point x $\widetilde{F}_{\text{drive}}(x,s)$:

$$\widetilde{F}(x,s)=\widetilde{F}_{\text{hydro}}(x,s)+\widetilde{F}_{\text{drive}}(x,s), \tag{5}$$

where

$$\widetilde{F}_{\text{hydro}}(x,s)=-\frac{\pi}{4}\rho_{\text{w}}\omega^2W^2\Gamma_1(\omega)w(x,s). \tag{6}$$

The expression of $\Gamma_1(\omega)$ can be found in ref. [28]. By substituting eqs. (5) and (6) into eq. (4) and rearranging, the beam dynamics equation is founded:

$$\frac{\partial^4w(x,s)}{\partial x^4}-\frac{\left(-\mu-\frac{\pi}{4}\rho_{\text{w}}W^2\Gamma_1(\omega)\right)L^4}{YI}s^2w(x,s)=\frac{\widetilde{F}_{\text{drive}}(x,s)}{YI}L^4. \tag{7}$$

For simplicity, eq. (7) can be rewritten as follows:

$$\frac{\partial^4w(x,s)}{\partial x^4}-B^4(s)w(x,s)=C(x,s), \tag{8}$$

where

$$B(s)=\left[\frac{\left(-\mu-\frac{\pi}{4}\rho_{\text{w}}W^2\Gamma_1(\omega)\right)L^4s^2}{YI}\right]^{1/4},$$

$$C(x,s)=\frac{\widetilde{F}_{\text{drive}}(x,s)}{YI}L^4.$$

To obtain the analytic solution of eq. (8), we use the theory of Green's functions [28]. Then the general solution to eq. (8) can be obtained as

$$w(x,s)=\int_0^1G(x,x',s)C(x',s)\mathrm{d}x', \tag{9}$$

where $G(x, x', s)$ is Green's function. Eq. (9) is the deflection function of the IPMC beam oscillating in a viscous fluid. Tan [18] gave a solution to a fourth-order partial, which also leads to the dynamic deflection $w(x, t)$ of the beam. Nevertheless, it contains infinite series and makes it complicated for simulation.

3.3 IPMC beam electrical actuation model

In this subsection, we will focus on solving the force and moment generated by IPMC actuation. Nemat-Nasser and Li [29] proposed the model that describes mechanoelectrical transduction considering electrostatic interaction within the polymer. The underlying cause of actuation was explained by the internal stress induced by interaction between ion pairs inside a cluster. Chen and Tan investigated the electrical dynamics of IPMC based on Nemat-Nasser's work [17]. They expanded the model and added the effect of surface resistance. Their model was represented as an infinite-dimensional transfer function relating the bending displacement $w(l, s)$ to the applied voltage $V(s)$. l is denoted as $l = x \times L$. As shown in Figure 2, the IPMC beam is clamped at one end $l = 0$ and is subject to an actuation voltage producing the tip displacement $w(L, t)$ at the other end $l = L$. The actuation-induced bending moment $M_{\text{IPMC}}(l,s)$ at point l could be expressed as

$$M_{\text{IPMC}}(l,s)=\frac{\alpha_0WK\kappa_{\text{e}}\left(\gamma(s)-\tanh\left(\gamma(s)\right)\right)}{\left(s\gamma(s)+K\tanh\left(\gamma(s)\right)\right)}\times\frac{\cosh\left(\sqrt{D(s)}l\right)-\sinh\left(\sqrt{D(s)}l\right)\tanh\left(\sqrt{D(s)}L\right)}{1+r_2\theta(s)}V(s), \tag{10}$$

where

$$K=\frac{F^2dC^-}{\kappa_{\text{e}}RT_{\text{a}}}\left(1-C^-\Delta V\right),$$

$$\gamma(s)=\sqrt{\frac{K+s}{d}}h,$$

$$\theta(s)=\frac{W\kappa_{\text{e}}s\gamma(s)(s+K)}{h\left(s\gamma(s)+K\right)},$$

$$D(s)=\sqrt{r_1\left(\frac{\theta(s)}{1+r_2\theta(s)}+\frac{2}{R_{\text{p}}}\right)}.$$

The moment $M_{\text{IPMC}}(l,s)$ induced by IPMC actuation can be replaced by two components: a distributed force density $F_{\text{d}}(x',s)$ acting along the length of the beam, and a moment $M(L_0,s)$ at the end of the beam, as shown in Figure 3 [18]. The deflection of the IPMC beam can be described as [30]

$$w(x,s)=\frac{L^4}{YI}\left(\int_0^1G(x,x',s)F_{\text{d}}(x',s)\mathrm{d}x'+M(L_0,s)\left.\frac{\partial G(x,x',s)}{\partial x'}\right|_{x'=1}\right). \tag{11}$$

3.4 Actuation model of the IPMC tail

We derive the analytic solution of $w(x,s)$ and the transfer function for the IPMC fish with hydro-fin in this subsection. Based on eqs. (10) and (11), the transfer function $R_1(L,s)=w(L,s)/V(s)$ can be obtained.

A passive plastic tail is attached to the end of the IPMC beam to achieve more thrust during the swimming state. Then, the thrust efficiency of IPMC fish with that tail is to be learned.

The passive fin is rigid compared to IPMC. The hydrodynamic force acting on the passive tail can be replaced by a concentrated moment $M_{\text{tail}}(s)$ acting at the end of the

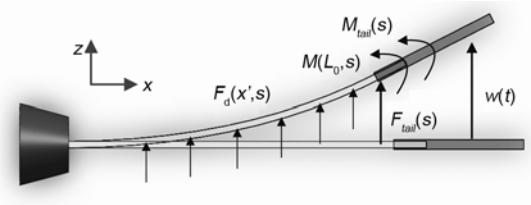

Figure 3 Illustration of replaced actuation force acting on the IPMC and hydro-force acting on the tail.

beam and a force $F_{\text{tail}}(s)$ acting at the end of the beam [18], as shown in Figure 3. The deflection $w(x,s)$ of the IPMC beam with passive tail is derived as

$$w(x,s) = \frac{L_0^4}{YI}\left(\begin{array}{l}\int_0^1 G(x,x',s)F_{\text{d}}(x',s)\text{d}x' + G(x,1,s)F_{\text{tail}}(s) \\ +\left(M_{\text{tail}}(s)+M(L_0,s)\right)\left.\dfrac{\partial G(x,x',s)}{\partial x'}\right|_{x'=1}\end{array}\right). \quad (12)$$

Through solving eq. (12), the desired transfer functions $R_2(L_0,s)=w(L_0,s)/V(s)$ and $R_{2\text{d}}(L_0,s)=w'(L_0,s)/V(s)$ are obtained. The transfer functions $R_3(L_1,s)$ and $R_{3\text{d}}(L_1, s)$ are donated as

$$R_3(L_1,s)=\frac{w(L_1,s)}{V(s)}=R_2(L_0,s)+R_{2\text{d}}(L_0,s)(L_1-L_0), \quad (13)$$

$$R_{3\text{d}}(L_1,s)=\frac{w'(L_1,s)}{V(s)}=R_{2\text{d}}(L_0,s). \quad (14)$$

Then eqs. (13) and (14) will be applied to the derivation of the robotic fish's thrust efficiency. Compared with Tan's work [18], the transfer function proposed in this paper contains only finite terms, which is more accurate and brief.

3.5 Thrust efficiency model of fish propulsion

Based on eqs. (1), (13) and (14), the speed U_{sim} of the IPMC fish under input voltage $V(t)=A_{\text{v}}\sin(\omega t)$ can be expressed as

$$U_{\text{sim}}=\sqrt{\frac{m^2\omega^2 A_{\text{v}}^2\left|R_3(L_1,j\omega)\right|^2}{2C_{\text{D}}\rho_{\text{w}}S+mA_{\text{v}}^2\left|R_{3\text{d}}(L_1,j\omega)\right|^2}}. \quad (15)$$

With eqs. (2), (13) and (14), the expression of the thrust efficiency η_{sim} of the IPMC fish can be derived further and becomes

$$\eta_{\text{sim}}=\frac{\omega^2\left|R_3(L_1,j\omega)\right|^2-U_{\text{sim}}^2\left|R_{3\text{d}}(L_1,j\omega)\right|^2}{2\left(\omega^2\left|R_3(L_1,j\omega)\right|^2+U_{\text{sim}}\omega\left|R_3(L_1,j\omega)\right|\left|R_{3\text{d}}(L_1,j\omega)\right|\right)}. \quad (16)$$

4 Parameters identification and experimental results

In this section, the parameters of the IPMC model (see eq. (10)) are identified through experiments. The IPMC material used in this paper is from Environmental Robots Inc., USA. Figure 4 shows the experiment setup for the identification of IPMC model. The IPMC beam was fixed at one end. A signal generator (YX1620P, Yangzhong Pioneer Electronics Co., China) with a power amplifier provided the actuation sinusoidal signals with amplitude 3.3 V and frequency from 0.1 to 20 Hz. The oscillation of IPMC beam was measured by a laser sensor (OADM 20U2441/S14C, Baumer Inc., Switzerland). A data recorder (Nicolet Vision XP, LDS Inc., Germany) was used to record the experiment results which has 16 sampling channels and a maximum sampling rate of 100 kHz. Based upon the actuation response of the IPMC beam, the magnitude and phase response of the actuator at frequency f can be obtained. Some parameters except physical parameters (e.g., R, F) and measured directly parameters (e.g., T_{a}, h, Y) need to be identified through curve-fitting using the least-square method [17]. The recorded experimental data were analyzed in a computer using MATLAB (http://www.mathworks.com/). Through least-square error analysis of the experimental data, the parameters were derived. Table 1 lists the parameters obtained for the IPMC actuation model and efficiency model. Two IPMC beams of different thicknesses and sizes were tested. The dimensions of IPMC beams are shown in Table 2. Figure 5 shows the comparison of IPMC actuation responses with model predictions for the two IPMC strips: Figure 5(a) is for IPMC 1 and Figure 5(b) is for IPMC 2. Generally, the magnitude and phase of the IPMC model show a nonlinear decrease as the actuation frequency increases. It is found that the magnitude gain and phase shift of the actuation model with the identified parameters are in good agreement with the experiment results.

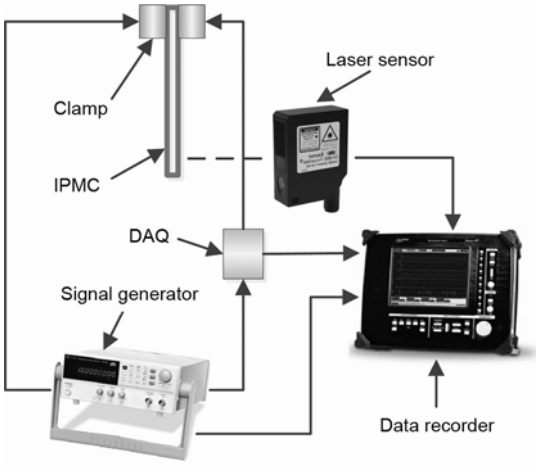

Figure 4 The experiment setup for the identification of IPMC model.

Table 1 Parameters for IPMC actuation model and efficiency model

Item	Value
F (C/mol)	96487
R (J/mol K)	8.3143
T_a (K)	297
R_p (Ω m)	24.9
Y (MPa)	90.92
r_1 (Ω m)	2210
r_2 (Ω m)	4.8×10^{-4}
d (m^2/s)	6.38×10^{-7}
C^- (mol/m^3)	1113
κ_e (F/m)	9.8×10^{-5}
α_0 (J/C)	0.135

Table 2 Dimensions of IPMC beams

Item	h (μm)	L (mm)	W (mm)
IPMC 1	175	26.6	6.2
IPMC 2	100	42.5	12

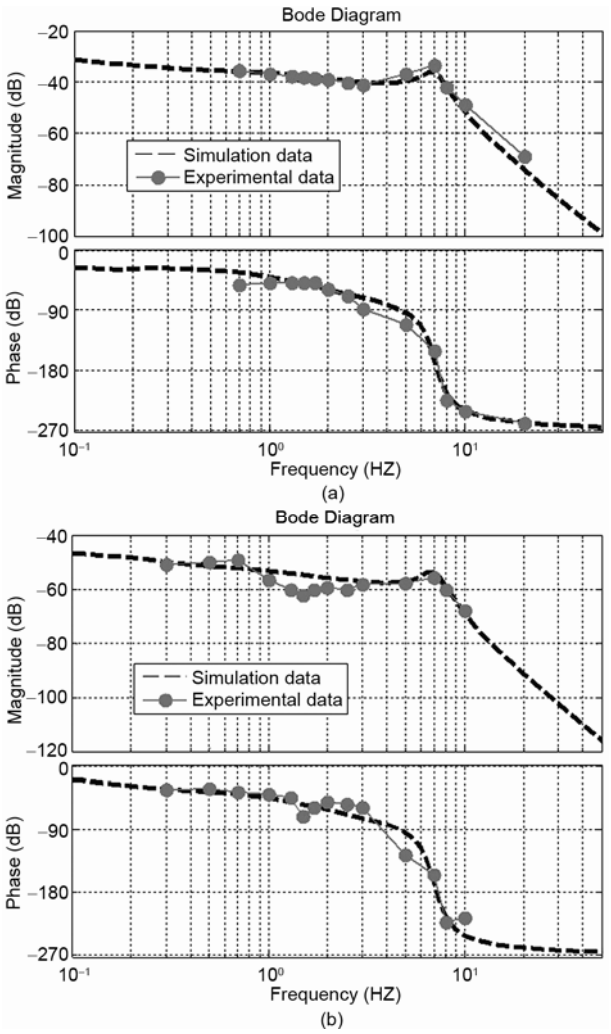

Figure 5 Comparison of IPMC actuation responses with actuation model predictions: (a) IPMC 1; (b) IPMC 2.

5 Hydrodynamic experimental test and model verification

In this section, we will test the thrust efficiency of the IPMC fish and compare the experimental data with the simulation result of the theoretical model. The thrust efficiency η_{exp} is donated as

$$\eta_{exp} = \frac{T_{exp} \cdot U_{exp}}{\overline{P}_{exp}}. \quad (17)$$

The thrust T_{exp}, speed U_{exp} and power consumption $\overline{P}_{exp}$ should be measured to obtain the experimental result of thrust efficiency. A series of experiments were conducted in a towing system and a water tank, as shown in Subsection 5.1. We would introduce the measurement method and results of U_{exp}, T_{exp} and $\overline{P}_{exp}$ in Subsections 5.2, 5.3 and 5.4 separately. Subsection 5.5 provides the final derivation of the thrust efficiency.

5.1 Experimental setup

First, we introduce the experimental method. The hydrodynamic experiment was conducted in a horizontal low-velocity servo towing system to ascertain the thrust efficiency. This servo towing system is driven by a 4000 W AC motor and has been used previously for the purpose of obtaining quantitative hydrodynamics of self-propulsion underwater robot [31–35]. The water tunnel has a running speed range from 0.005 to 1 m/s, and the uniformity of the flow velocity is 0.2%.

Figure 6 shows the mechanical components of a self-propelled experimental apparatus, where the robotic fish and its affiliated components are fixed vertically under a component force transducer (CFBLSM, BGTSE Inc., China) which is attached to the carriage by screws. The robotic fish is submerged under water, while its transmission mechanism is mounted on a metal plate and is above the surface of the water. The force T (see Figure 6) is measured using the force transducer which has a measuring range of 1 N and a sensitivity of 0.01 N in the axial direction. A low resistance bearing is set at the joint. According to the lever principle, the resultant force on the fish is amplified by 100 times when it is transferred to the force sensor. Thus, the external force T_{ext} from the external apparatus acting on the fish could be measured by $T_{ext} = T/100$. The center of mass G of the fish is set right under the mast to minimize the influence of gravity during the experiments.

The control unit and power supply of the robotic fish are both mounted on a carriage rest which is belt-driven on rails that run along the towing direction (the forward direction). The water tank, which is 7.8 m × 1.2 m × 1.1 m, is filled with water, and provides the robotic fish with sufficient space to move without being affected by the boundaries on

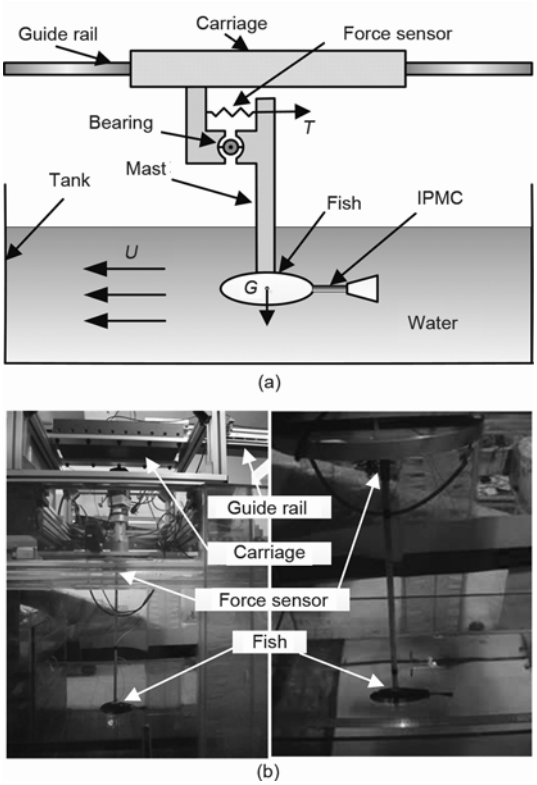

Figure 6 Experiment setup: (a) Illustration of the thrust measurement system; (b) Snapshot of the water tunnel and the fish thrust measurement system.

both sides. The fish is also located at mid-depth in the tank to avoid any interferences from the free surface and the bottom of the tank. Currently we just consider the forward direction of fish swimming with the lateral and rotational direction constraint. This simplified method (e.g. lateral constraint and rotational direction) is widely employed in both experimental and numerical hydrodynamic research of fish swimming just considering the straight-line swimming [25, 36]. We used Nicolet Vision XP to record the experimental data.

5.2 Swimming speed

Experiments were performed to test the speed of the robotic fish, which is a significant part in the thrust performance. In this experiment, the robotic fish propelled by the IPMC tail was tested by swimming freely in the tank, and a timer was used to record the time during which the fish travelled at the steady state through a given distance of 10 cm. The velocities of the robotic fish were measured under sinusoidal wave voltage inputs with amplitude $A_v = 3.3$ V and different frequencies. Figure 7 shows a snapshot of the fish swimming in the tank. Under each actuated frequency, the fish swimming performance was repeated 5 times and the cruising speed U_{exp} was obtained by the average.

The capability of the model in predicting the cruising speed (see eq. (15)) of the IPMC fish was validated under different operating frequencies. Two hybrid tails of different IPMCs were investigated, shown in Table 3. It can be found that the predicted speeds matched the experimental data well, as shown in Figure 8. For each tail, there was an opti-

Table 3 Dimensions of IPMC tails (see Figure 2 for the definitions of dimension variables)

Item	L_0 (mm)	L_1 (mm)	b_0 (mm)	b_1 (mm)
IPMC 1	23.6	56.6	6	24
IPMC 2	42.5	64.6	6	24

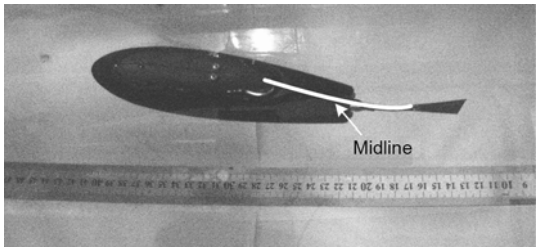

Figure 7 Snapshot of IPMC fish swimming in the tank.

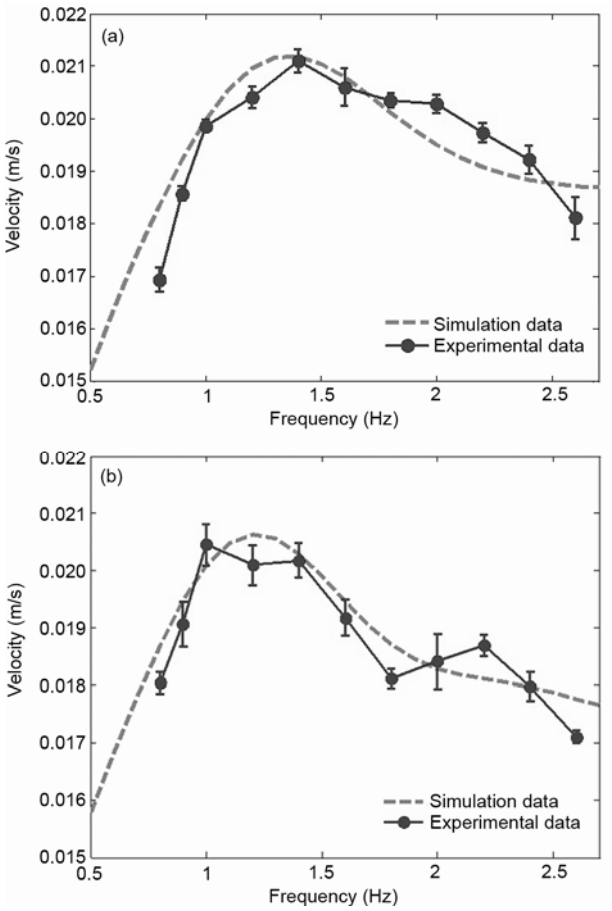

Figure 8 Comparison of experimental IPMC fish speed data with model predictions: (a) with IPMC 1; (b) with IPMC 2.

mal frequency that approximated 1.4 Hz under which the fish reached the highest speed. The speed data has a good agreement with the results in refs. [18] and [20]. As the actuation frequency becomes relatively high or low, the speed of the IPMC fish decreases. The model can well predict the speed of the robotic fish with different IPMC tail dimensions.

5.3 Thrust force

In this subsection, we studied the thrust force and drag coefficient of the IPMC fish through hydrodynamic experiments. Since the thrust force could not be measured directly when the robotic fish was swimming because its thrust and drag were combined together, the thrust force propelled by the IPMC was measured in the towing system. It should be noted that in most conventional dragging hydrodynamic experimental methods of robotic model, the force $T_{ext} \neq 0$ along the forward direction, which means the thrust force is not equal to the drag force [37–41]. As a result, the external force was absorbed by the external apparatus. Thus, the robotic fish was not self-propelled, but moved at a constrained imposed flow, and there was no equality between the thrust and drag force. Taking both the active and passive towing approaches into consideration, a novel experimental approach combining the advantages of both methods was proposed.

The robotic fish was towed under the servo towing system at towing speeds shown in Figure 8 for different tails. For each cruising speed U_{exp}, the IPMC was under corresponding sinusoidal wave voltage input. There might be some interference (e.g., the fish not swimming straightly, and the inaccuracy of human using a timer to record time) on the measuring of the cruising speed U_{exp} in Subsection 5.2. We adjusted the towing speed during the drag experiment to ensure the external force $T = 0$. According to the Newton's law, the robotic fish was considered to swim freely without any external force acting on it from the apparatus when the detected force $T = (F_D - T_{exp}) \times 100 = 0$, where the drag force F_D was equal to the thrust force T_{exp}. The range of IPMC fish swimming under the self-propelled condition in the drag experiment was 70 cm. Overall, more than one hundred groups of tests were conducted.

The thrust force T_{exp} would be measured next. When the fish swam under the speed U_{exp}, we could gain T_{exp} by measuring the drag force F_D. To obtain the drag force F_D, the input voltage of IPMC was set zero. Through towing the fish under the system at U_{exp}, the F_D was measured. In this paper, the drag experiments were conducted three times for each cruising speed U_{exp}, to ensure the repeatability and accuracy of the test result. More than seventy runs were done.

Figure 9 shows the experimental thrust force comparison of the IPMC fish with different tails. The thrust produced by the IPMC tail reached its maximum when the frequency approximated 1.4 Hz, which is in good agreement with the speed of IPMC fish shown in Figure 8. It also showed in the experiments that the thrust can be improved by increasing the actuator length as well as the maximum tip displacement, as indicated in ref. [21].

The drag coefficient C_D, as a significant parameter in the theoretical model, is related to the fish body that depends on the Reynolds number, the fitness ratio of the body, and the properties of the fish surface. The drag force is defined as

$$F_D = \frac{C_D \cdot \rho_w \cdot U^2 \cdot S}{2}. \tag{18}$$

In order to identify C_D, the fish was towed at different towing speeds U ranging from 0.005 to 0.1 m/s. More than fifty experiments were done. With the measured drag force F_D, velocity U, and surface area of the fish S, the drag coefficient C_D was derived. Table 4 shows the parameters of the drag experiment.

5.4 Power consumption

To obtain the power output of the robotic fish in fluid during swimming state, we need to test the power consumption of the IPMC tail under different circumstances. Firstly, the IPMC tail oscillated in water under the corresponding voltage input in Subsection 5.2. The tip displacement D_{flu} was measured using the laser sensor. An oscilloscope was used to graph D_{flu}. Figure 10 gives a schematic view of the power consumption measurement apparatus. The simultaneous input voltage and output current as well as the D_{flu} were recorded. Then, the IPMC tail oscillated in air under

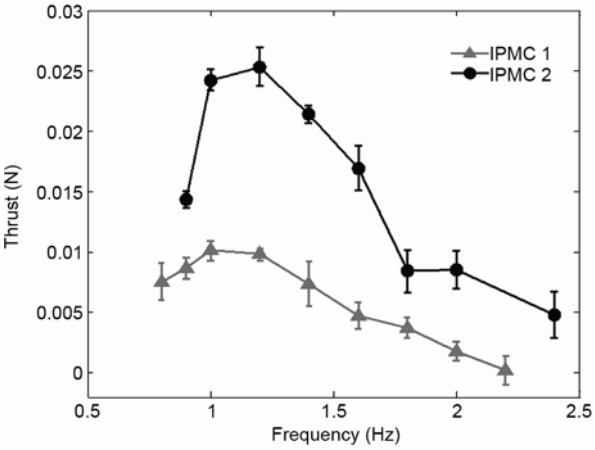

Figure 9 Experimental thrust force comparison of IPMC fish with different tails.

Table 4 Parameters of the drag experiment

S (m^2)	C_D	ρ_w (kg/ m^3)
0.0173	0.046	1000

the same voltage input. Based on the display of the oscilloscope, the amplitude of the voltage output from the amplifier was adjusted to maintain the consistent nominal displacement amplitude of D_{flu} in air with the corresponding frequency. During IPMC vibrated underwater and in air, the voltages U_{flu}, U_{air} and currents I_{flu}, I_{air} were measured. The average power that the IPMC outputs in the fluid during one cycle at frequency f can be obtained as

$$\overline{P}_{\text{exp}} = \frac{1}{1/f}\int_{t_s}^{t_s+1/f}\left(U_{\text{flu}}I_{\text{flu}} - U_{\text{air}}I_{\text{air}}\right)\mathrm{d}t, \tag{19}$$

where t_s is a random point in time during IPMC operating. Finally, $\overline{P}_{\text{exp}}$ including the power used to propel the robotic fish and wasted in the water was obtained.

In this experiment, a dynamic measurement calibration method was used in order to ensure the displacement measurement's precision. The result of the final dynamic displacement calibration showed that the amplitude error is within 5%. It was found that under the same voltage input, the deflection of the IPMC in air operation is larger than the deflection in water operation, which was discussed in ref. [42]. Figure 11 gives a comparison of IPMC tail power consumptions, applied voltages and current outputs with the same amplitude in air and underwater at the frequency of 1 Hz. The IPMC tails were tested under different frequencies. Figure 12 gives the power outputs of the two IPMC tails in the fluid. It can be seen that with the operating frequency increasing, the power output of the IPMC tail increases significantly. Considering the result of the speed and thrust force of IPMC fish decreases as the frequency is relatively high (Figures 8 and 9), it might be inferred that there is some optimal point of the thrust efficiency when the frequency is relatively low. It was also noticed that during the experiment the amplitude of IPMC tail showed an overall decrease underwater as the frequency increased.

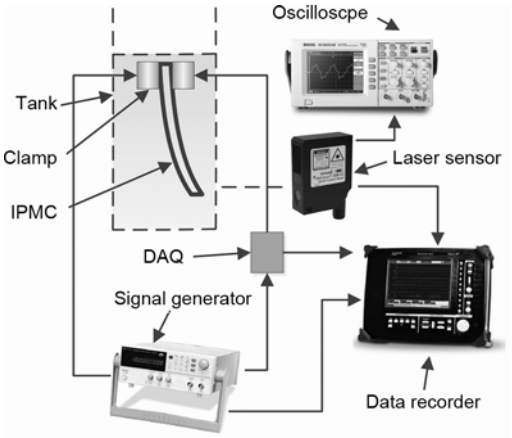

Figure 10 Schematic view of the power consumption measurement apparatus.

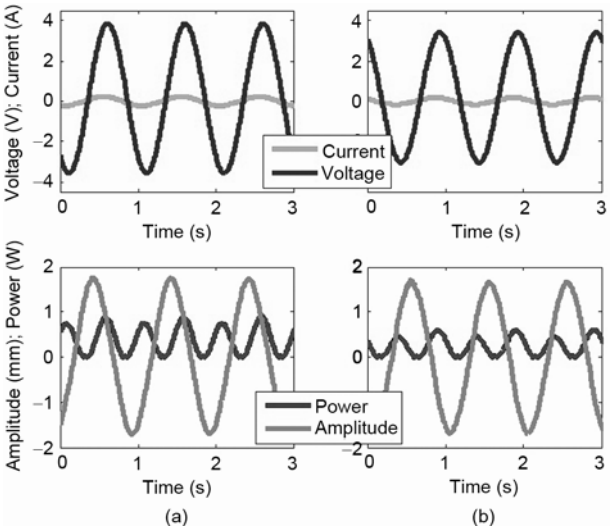

Figure 11 Comparison of experimental IPMC tail power consumptions, applied voltages and current outputs with the equivalent vibrating amplitude at the frequency of 1 Hz: (a) IPMC vibrating underwater; (b) IPMC vibrating in air.

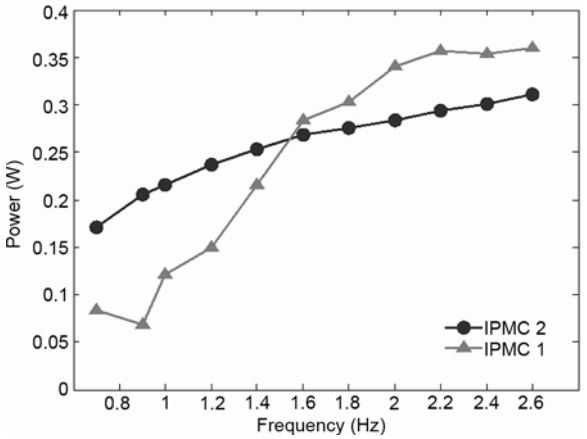

Figure 12 Power output of different IPMC tails in the fluid.

5.5 Thrust efficiency

Finally, we derived the experimental thrust efficiency of the IPMC fish. Based on the measured thrust force T_{exp}, speed U_{exp}, power consumption $\overline{P}_{\text{exp}}$ and with eq. (17), the experimental data of the IPMC fish thrust efficiency η_{exp} was obtained.

The capability of the efficiency model (see eq. (16)) in predicting efficiency was verified for different operating frequencies. It was simulated for different tail dimensions: Figure 13(a) is for IPMC 1 and Figure 13(b) is for IPMC 2. It is shown that the simulation result of the efficiency model η_{sim} matches well with the experiment data η_{exp}. It can be seen that firstly, the efficiency increases as the frequency increases, and with the frequency being relatively high, the efficiency decreases. Its thrust efficiency reaches the maximum when the frequency is approximately 1.1 Hz. The

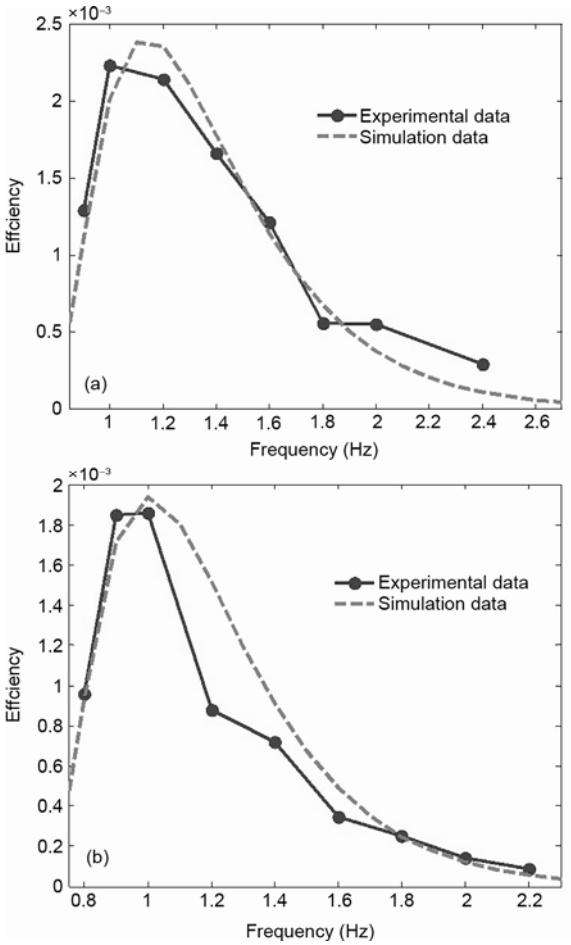

Figure 13 Comparison of experimental IPMC fish efficiency data with model predictions: (a) with IPMC 1; (b) with IPMC 2.

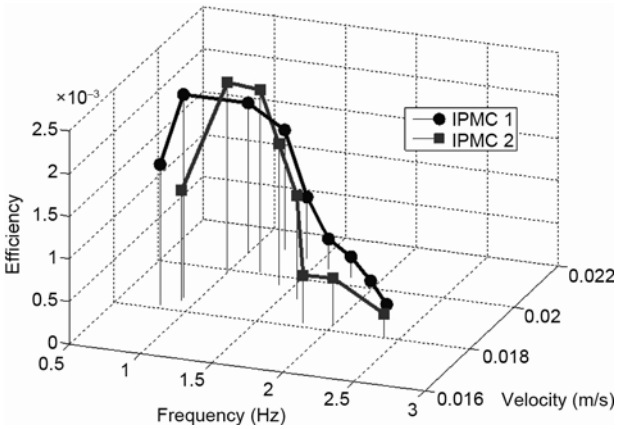

Figure 14 A 3D plot showing the comparison of efficiencies and velocities in various actuation frequencies for different IPMCs.

thrust efficiency of the IPMC fish varies with different tails, and each has its optimal frequency. The model can well predict the thrust efficiency of the IPMC fish and provides the principle for optimal design and control of the high efficient robotic fish propelled by IPMC.

Figure 14 gives a 3D plot showing the comparison of thrust efficiencies and velocities of IPMC fish at different actuation frequencies. It is found that the fish could obtain high thrust efficiency when its actuation frequency is approximately 1 Hz, which could gain a relatively high speed simultaneously. We may consider that the IPMC fish could achieve a good swimming performance in terms of both speed and thrust efficiency when its actuation frequency is close to the one corresponding to the optional point for the speed.

6 Concluding remarks and future studies

In small underwater robots, the thrust performance is important due to their limited energy. In this paper, we proposed a model that predicts the thrust efficiency of an IPMC actuated fish and we experimentally measured its thrust efficiency. The model incorporates both hydrodynamics and actuation dynamics of IPMC. Using a servo towing system, a novel experimental approach was developed and the model has been experimentally verified with different IPMCs. The measurement of thrust efficiency of the robotic fish was completed under the self-propelled conditions.

Comparison between the theoretical model and experimental results shows that the theoretical model can well predict the thrust efficiency of the robotic fish under different actuation frequencies. When the optimal actuation frequency increases or decreases by 20%, the thrust efficiency decreases by 50%. The robotic fish has an optimal actuation frequency for the thrust efficiency, which showed relatively good agreement with the optimal point for the self-propelled speed. Moreover, it is interesting that the peak measured efficiency of IPMC fish was 2.3×10^{-3}, recorded at 1 Hz, and the optimal actuation frequency for the thrust efficiency approximated that for the cruising speed. The peak thrust force was 0.025 N, recorded at 1.2 Hz, showing a good agreement with the speed. The maximum value of speed was 0.021 m/s at 1.5 Hz. A peak power of 0.36 W was recorded at 2.6 Hz, which illustrates the relatively high power consumption of IPMC. In particular, the parameters were derived through fundamental character of IPMC so the model is feasible in practical application. The theoretical model provides a method to analyze the underwater robots. The servo towing system and the self-propelled approach also offer a platform to experimentally study the thrust efficiency of underwater robots actuated by other types of smart material.

In our work, we considered that the plastic fin attached to the IPMC is rigid in the fluid. Meanwhile we do not consider its mass. According to previous work, when compared to a rigid flapping foil, the thrust efficiency of a two-dimensional flapping foil with chord-wise flexibility is experimentally shown to increase significantly, i.e., up to 36% [36]. In our future work, we will focus on the influence of a soft fin on the swimming performance of the

IPMC propelled robotic fish. Future work will also include the efficient control strategy for bionic IPMC fish and extend the efficiency model for different Reynolds number circumstances so as to study the fish thrust performance in varied scale.

Many thanks to CHEN Yang, BAO Lei and SHI ZhenYun for helping to improve this paper. This work was supported by the National Natural Science Foundation of China (Grant No. 61075100).

1 Mason R, Burdick J W. Experiments in carangiform robotic fish locomotion. Proc of the IEEE Int Conf on Robotics & Automation, 2000, 1. New York: IEEE. 428–435
2 Zhou C L, Low K H. Design and locomotion control of a biomimetic underwater vehicle with fin propulsion. IEEE/ASME T Mech, 2012, 17(1): 25–35
3 Arash T, Sakineh O. A novel miniature virus-inspired swimming robot for biomedical applications. Sci China Tech Sci, 2010, 53(11): 2883–2895
4 Zhou C, Cao Z Q, Wang S, et al. A marsupial robotic fish team: Design, motion and cooperation. Sci China Tech Sci, 2010, 53(11): 2896–2904
5 Morgansen K A, Triplett B I, Klein D J. Geometric methods for modeling and control of free-swimming fin-actuated underwater vehicles. IEEE T Robot, 2007, 23(6): 1184–1199
6 Yu J, Tan M, Wand S, et al. Development of a biomimetic robotic fish and its control algorithm. IEEE T Syst Man Cy, 2004, 34(4): 1798–1810
7 Borgen M G, Washington G N, Kinzel G L. Design and evolution of a piezoelectrically actuated miniature swimming vehicle. IEEE/ASME T Mech, 2003, 8(1): 66–76
8 Rossi C, Coral W, Colorado J, et al. A motor-less and gear-less bio-mimetic robotic fish design. Proc of the IEEE Int Conf on Robotics & Automation, 2011. New York: IEEE. 3646–3651
9 Tangorra J, Anquetil P, Fofonoff T, et al. The application of conducting polymers to a biorobotic fin propulsor. Bioinsp Biomimet, 2007, 2: 6–17
10 Shahinpoor M, Kim K J. Ionic polymer-metal composites: I. Fundamentals. Smart Mater Struct, 2001, 10: 819–833
11 Shahinpoor M, Kim K J. Ionic polymer-metal composites: IV. Industrial and medical applications. Smart Mater Struct, 2005, 14: 197–214
12 Shahinpoor M. Conceptual design, kinematics and dynamics of swimming robotic structures using ionic polymeric gel muscles. Smart Mater Struct, 1992, 1(1): 91–94
13 Takagi K, Yamamura M, Luo Z W, et al. Development of a Rajiform Swimming Robot using Ionic Polymer Artificial Muscles. Proc of the IEEE/RSJ Int Conf on Intelligent Robots & Systems, 2006. New York: IEEE. 1861–1866
14 Anton M, Punning A, Aabloo A M, et al. Towards a biomimetic EAP Robot. Proc of Towards Autonomous Robotic Systems, 2004. 6–8
15 Yamakita M, Kamamichi N, Kozuki T, et al. A snake-like swimming robot using IPMC actuator and verification of doping effect. Proc of the IEEE/RSJ Int Conf on Intelligent Robots & Systems, 2005. New York: IEEE. 3333–3338
16 Yim W, Lee J, Kim K J. An artificial muscle actuator for biomimetic underwater propulsors. Bioinsp Biomimet, 2007, 2: 31–41
17 Chen Z, Tan X B. A control-oriented and physics-based model for ionic polymer-metal composite actuators. IEEE/ASME T Mech, 2008, 13(5): 519–529
18 Chen Z, Shatara S, Tan X B. Modeling of biomimetic robotic fish propelled by an ionic polymer-metal composite caudal fin. IEEE/ASME T Mech, 2010, 15(3): 448–459
19 Mbemmo E, Chen Z, Shatara S, et al. Modeling of biomimetic robotic fish propelled by an ionic polymer-metal composite actuator. Proc of the IEEE Int Conf on Robotics & Automation, 2008. New York: IEEE. 689–694
20 Aureli M, Kopman V, Porfiri M. Free-locomotion of underwater vehicles actuated by ionic polymer metal composites. IEEE/ASME T Mech, 2010, 15: 603–614
21 Abdelnour K, Mancia E, Peterson S D, et al. Hydrodynamics of underwater propulsors based on ionic polymer metal composites: A numerical study. Smart Mater Struct, 2009, 18: 085006
22 Peterson S D, Porfiri M, Rovardi A. A particle image velocimetry study of vibrating ionic polymer metal composites in aqueous environments. IEEE/ASME T Mech, 2009, 14(4): 474–483
23 Lighthill M J. Note on the swimming of slender fish. J Fluid Mech, 1960, 9: 305–317
24 Ohlberger J, Staaks G, Holker F. Swimming efficiency and the influence of morphology on swimming costs in fishes. J Comp Physiol B, 2006, 176: 17–25
25 Barrett D, Triantafyllou M, Yue D, et al. Drag reduction in fish-like locomotion. J Fluid Mech, 1999, 392: 183–212
26 Schultz W W, Webb P W. Power requirements of swimming: Do new methods resolve old questions? Integr Comp Biol, 2002, 42: 1018–1025
27 Landau L D, Lifshitz E M. Theory of Elasticity. Pergamon: Oxford Press, 1970
28 Sader J E. Frequency response of cantilever beams immersed in viscous fluids with applications to the atomic force microscope. J Appl Phys, 1998, 84(1): 64–76
29 Nemat-Nasser S, Li J. Electromechanical response of ionic polymer-metal composites. J Appl Phys, 2000, 87(7): 3321–3331
30 Lu P, Lee K. An alternative derivation of dynamic admittance matrix of piezoelectric cantilever bimorph. J Sound Vib, 2003, 266: 723–735
31 Wen L, Wang T M, Wu G H, et al. A novel method based on a force-feedback technique for the hydrodynamic investigation of kinematic effects on robotic fish. Proc of the IEEE Int Conf on Robotics & Automation, 2011. New York: IEEE. 203–208
32 Wen L, Wang T M, Liang J H, et al. Novel method for modeling and control investigation of efficient-swimming carangiform robotic fish. IEEE/ASME T Ind Electron, 2012, 59(8): 3176–3188
33 Wen L, Wang T M, Wu G H, et al. Experimental method and instrumentation for the measurement of thrust efficiency of a self-propulsion robotic fish. IEEE/ASME T Mech, 2012, DOI: 10.1109/TMECH.2012.2194719
34 Wen L, Wang T M, Wu G H, et al. Hydrodynamic investigation of a self-propulsive robotic fish based on a force-feedback control method. Bioinspir. Biomim, 2012, 7: 036012
35 Wen L, Wang T M, Wu G H, et al. Hybrid undulatory kinematics of a robotic mackerel (Scomber scombrus): Theoretical modeling and experimental investigation. Sci China Tech Sci, 2012, 55: 2941–2952
36 Prempraneerach P, Hover F, Triantafyllou M. The effect of chordwise flexibility on the thrust and efficiency of a flapping foil. Proc of the 13th Int Symposium on Unmanned Untethered Submersible Technology. Durham, USA, 2003. 120–128
37 Bandyopadhyay P R. Trends in biorobotic autonomous undersea vehicles. IEEE J Ocean Eng, 2005, 30: 109–139
38 Beal D N, Hover F S, Triantafyllou M S, et al. Passive propulsion in vortex wakes. J Fluid Mech, 2006, 549: 385–402
39 Tan G K, Shen G X, Huang S Q. Investigation of flow mechanism of a robotic fish swimming by using flow visualization synchronized with hydrodynamic force measurement. Exp Fluids, 2007, 43: 811–821
40 Brucker C, Bleckmann H. Vortex dynamics in the wake of a mechanical fish. Exp Fluids, 2007, 43: 799–810
41 Tangorra J, Anquetil P, Fofonoff T, et al. The application of conducting polymers to a biorobotic fin propulsor. Bioinsp Biomimet, 2007, 2: 6–17
42 Dogruer D, Lee J, Yim W, et al. Fluid interaction of segmented ionic polymer-metal composites under water. Smart Mater Struct, 2007, 16: 220–226